Article

Excitation Energy Transport Processes of Porphyrin Monomer, Dimer, Cyclic Trimer, and Hexamer Probed by Ultrafast Fluorescence Anisotropy Decay

Hyun Sun Cho, Hanju Rhee, Jae Kyu Song, Chang-Ki Min, Masayoshi Takase, Naoki Aratani, Sung Cho, Atsuhiro Osuka, Taiha Joo, and Dongho Kim

J. Am. Chem. Soc., **2003**, 125 (19), 5849-5860• DOI: 10.1021/ja021476g • Publication Date (Web): 19 April 2003

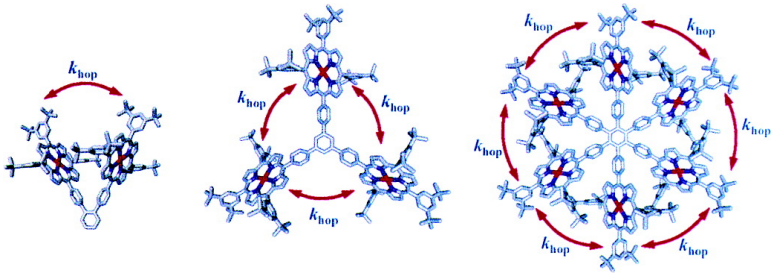

More About This Article

Additional resources and features associated with this article are available within the HTML version:

- Supporting Information
- Links to the 13 articles that cite this article, as of the time of this article download
- Access to high resolution figures
- Links to articles and content related to this article
- Copyright permission to reproduce figures and/or text from this article

View the Full Text HTML

J|A|C|S
ARTICLES
Published on Web 04/19/2003

Excitation Energy Transport Processes of Porphyrin Monomer, Dimer, Cyclic Trimer, and Hexamer Probed by Ultrafast Fluorescence Anisotropy Decay

Hyun Sun Cho,[†] Hanju Rhee,[‡] Jae Kyu Song,[†] Chang-Ki Min,[‡] Masayoshi Takase,[§] Naoki Aratani,[§] Sung Cho,[†] Atsuhiro Osuka,*[,§] Taiha Joo,*[,‡] and Dongho Kim*[,†]

Contribution from the National Creative Research Initiatives Center for Ultrafast Optical Characteristics Control and Department of Chemistry, Yonsei University, Seoul 120-749, Korea, Department of Chemistry, Pohang University of Science and Technology, Pohang, 790-784, Korea, and Department of Chemistry, Graduate School of Science, Kyoto University, Kyoto 606-8502, Japan

Received December 24, 2002; E-mail: dongho@yonsei.ac.kr

Abstract: Femtosecond fluorescence anisotropy measurements for a variety of cyclic porphyrin arrays such as Zn^{II}porphyrin *m*-trimer and hexamer are reported along with *o*-dimer and monomer as reference molecules. In the porphyrin arrays, a pair of porphyrin moieties are joined together via triphenyl linkage to ensure cyclic and rigid structures. Anisotropy decay times of the porphyrin arrays can be well described by the Förster incoherent excitation hopping process between the porphyrin units. Exciton coupling strengths of 74 and 264 cm^{-1} for the *m*-trimer and hexamer estimated from the observed excitation energy hopping rates are close to those of B800 and B850, respectively, in the LH2 bacterial light-harvesting antenna. Thus, these cyclic porphyrin array systems have proven to be useful in understanding energy migration processes in a relatively weak interaction regime in light of the similarity in overall structures and constituent chromophores to natural light-harvesting arrays.

Introduction

Numerous research activities have been directed toward unveiling energy transport phenomena occurring in natural light-harvesting complexes.[1,2] At the same time, the mimicry of natural light-harvesting machines has been continuously attempted by the design and synthesis of various types of covalently linked porphyrin arrays with the goal of applying these arrays to molecular photonic devices and artificial light-harvesting array systems.[3−13] One of the attractive features of this approach is a fine control of molecular structures in regular and well-arranged architectures. Thus, the motivation for the investigation of energy transport phenomena in porphyrin arrays has been promoted by the prospect of producing artificial light-harvesting systems as well as molecular photonic devices. A fundamental challenge in the photophysics of porphyrin array is the elucidation of the excitation energy transfer (EET) between porphyrin chromophores and the degree of the excitation delocalization. Depending on the strength of exciton coupling, the energy transfer lies in the strong coupling limit (coherent), weak coupling limit (hopping), or intermediate regime.[14] Thus, the interconnection length and the relative configuration between adjacent pigments are important to gain further insight into the exciton coupling dynamics and energy migration processes of porphyrin arrays especially in relation to natural light-harvesting array systems.

In bacterial photosynthetic systems such as *Rhodobacter sphaeroides*, two different types of antenna complexes exist: a core light-harvesting antenna (LH1) and a peripheral light-harvesting antenna (LH2).[15] The reaction center,[16] where a series of photoinduced electron-transfer reactions occur, is surrounded by the LH1. The peripheral antenna LH2 of photosynthetic purple bacteria forms two wheel-like structures: B800 with 9 bacteriochlorophyll *a* (Bchl *a*) molecules and B850 with 18 Bchl *a* molecules. The structural complexity in the circular arrangement of 18 Bchl *a* is that they are not evenly distributed. They

[†] Yonsei University.
[‡] Pohang University of Science and Technology.
[§] Kyoto University.

(1) Sundström, V.; Pullerits, T.; van Grondelle, R. *J. Phys. Chem. B* **1999**, *103*, 2327.
(2) Hu, X.; Ritz, T.; Damjanovic, A.; Autenrieth, F.; Schulten, K. *Q. Rev. Biophys.* **2002**, *35*, 1.
(3) Holten, D.; Bocian, D. F.; Lindsey, J. S. *Acc. Chem. Res.* **2002**, *35*, 57.
(4) Wagner, R. W.; Lindsey, J. S. *J. Am. Chem. Soc.* **1994**, *116*, 9759.
(5) Wagner, R. W.; Lindsey, J. S.; Seth, J.; Palaniappan, V.; Bocian, D. F. *J. Am. Chem. Soc.* **1996**, *118*, 3996.
(6) Gust, D.; Moore, T. A.; Moore, A. L. *Acc. Chem. Res.* **2001**, *34*, 40.
(7) Gust, D.; Moore, T. A.; Moore, A. L. *Acc. Chem. Res.* **1993**, *26*, 198.
(8) Liddell, P. A.; Kuciauskas, D.; Sumida, J. P.; Nash, B.; Nguyen, D.; Moore, A. L.; Moore, T. A.; Gust, D. *J. Am. Chem. Soc.* **1997**, *119*, 1400.
(9) Kodis, G.; Liddell, P. A.; de la Garza, L.; Clausen, P. C.; Lindsey, J. S.; Moore, A. L.; Moore, T. A.; Gust, D. *J. Phys. Chem. A* **2002**, *106*, 2036.
(10) Wasielewski, M. R. *Chem. Rev.* **1992**, *92*, 435.
(11) Debreczeny, M. P.; Svec, W. A.; Marsh, E. M.; Wasielewski, M. R. *J. Am. Chem. Soc.* **1996**, *118*, 8174.
(12) Debreczeny, M. P.; Svec, W. A.; Wasielewski, M. R. *Science* **1996**, *274*, 584.
(13) Vincent, M. G. H.; Jaquinod, L.; Smith, K. M. *Chem. Commun.* **1999**, 1771.
(14) Kimura, A.; Kakitani, T.; Yamato, T. *J. Phys. Chem. B* **2000**, *104*, 9276.
(15) Jungas, C.; Ranck, J.; Rigaud, J.; Joliot, P.; Vermeglio, A. *EMBO J.* **1999**, *18*, 534.
(16) Ermler, U.; Fritzsch, G.; Buchanan, S.; Michel, H. *Structure* **1994**, *2*, 925.

are composed of nine Bchl *a* dimeric forms with the Mg−Mg intradimer distance of 8.7 Å bound to the same $\alpha\beta$ polypeptide unit, whereas it is 9.7 Å between the adjacent dimeric units. The remaining nine Bchl *a* in B800 are located between the β-apoproteins, and the Mg−Mg distance between B800 Bchl *a* is 21 Å; that is, Bchl *a* in B800 may be regarded as monomers.

While Bchl *a* in B800 are only weakly interacting, those in B850 are strongly coupled to form exciton states as a consequence of the close face-to-face arrangement. The EET from B800 to B850 takes place rapidly with a time of 0.7−0.9 ps at room temperature.[1,17,18] The possibility of energy transfer between the excitonic states in B850 was discussed to account for the ultrafast ∼20-fs dynamics seen in the transient absorption.[19,20] Time-resolved fluorescence anisotropy measurement yields a single-step energy-transfer time scale of ∼100 fs among Bchl *a* in B850.[21] Femtosecond anisotropy measurements revealed that there is a fast energy transfer among B800 molecules with a time constant of 0.8−1.6 ps.[22] The excitation transfer was described as incoherent hopping in a system of spectrally inhomogeneous antenna molecules using a master equation approach.[23] A simulation showed that the measured B800 dynamics is well described as the characteristic energy transfer between the nearest-neighbor pairs with the transfer time of 0.35 ps among ∼10 Bchl *a* molecules in a circular arrangement.

Up to now, most of porphyrin arrays to mimic the natural photosynthetic systems have been prepared based on linear arrangement.[24−26] Circular arrangement of porphyrin moieties in a regular and rigid manner is indispensable for the mimicry of the LH1 and LH2 arrays in view of geometry. Besides the circular arrangement, our porphyrin array model systems are well suited in mimicking the LH1 and LH2 energy migration processes, because the oscillator strengths of the B-bands are comparable to those of the large Q_y electronic transitions of Bchl *a* in the LH1 and LH2 and the Stokes shifts for B-bands, which play a key role in determining a spectral overlap integral, are very small just like Bchl *a* in the LH1 and LH2. As a consequence, the contribution by vibronic bands, which leads to an overestimation of the Förster-type energy-transfer rate, is minimized because the spectral overlap is evaluated as a means of quantifying the role of vibrations in the energy transfer.

It has been demonstrated that the time-resolved fluorescence (TRF) provides the most unambiguous results on the excited-state dynamics, because more frequently employed transient absorption measurement is complicated due to multiple contributions by ground-state bleaching, excited-state absorption, and stimulated emission processes. Moreover, the fluorescence anisotropy decay is very informative in the investigation of intramolecular EET, in particular multichromophore systems, since the energy transfer is followed by the reorientation of the transition dipole, resulting in depolarization of the emission dipole.

There have been a few previous works on the photophysics of cyclic multiporphyrin arrays such as a hexameric benzoporphyrin and multiporphyrin dendrimers.[27−30] In the former, transient absorption measurement was used to show a ∼20-ps energy transport due to an intramolecular inter-porphyrin excited process, although rigid circular structure was enforced because of the relatively short linker connecting six porphyrin units. The EET processes in porphyrin dendrimers investigated by TRF anisotropy measurements indicate that the EET processes occur between chromophores within the dendrimers. But the picosecond fluorescence anisotropy measurements were focused on the S_1 state energy transport. More importantly, flexible and long dendrimers do not provide a rigid environment for the porphyrin chromophores to reside at restrictive positions to ensure the rigid and cyclic arrangement of the chromophores.

In this regard, we have synthesized a porphyrin array arranged in a cyclic manner to mimic the LH2 antenna system (Scheme 1), and interunit and intraunit energy-transfer processes have been measured by TRF. To elucidate the mechanism of energy transfer, several model compounds with a given geometry have also been synthesized and studied by femtosecond TRF. To the best of our knowledge, our study is the first attempt to examine ultrafast EET processes of cyclic porphyrin arrays bearing a close resemblance to the LH1 and LH2 arrays held in an $\alpha\beta$ polypeptide and carotene scaffold in overall structures and their constituent pigments (porphyrins vs bacteriochlorophylls).

Experimental Section

The time-resolved spontaneous fluorescence apparatus has been described in detail elsewhere.[31] In brief, the femtosecond light source was based on a home-built cavity-dumped Kerr lens mode-locked Ti: sapphire laser generating 15-fs pulses tunable in the near-infrared region. The second harmonic of the fundamental generated in a 100-μm-thick BBO crystal served as a pump pulse. Residual fundamental pulse was used as a gate pulse. Three pairs of fused-silica Brewster angle prisms compensate group velocity dispersions of the fundamental pulse prior to the second harmonic generation, the second harmonic around 400 nm, and the residual fundamental pulses.

In this work, emissions from the B (S_2) and Q (S_1) bands of the porphyrin arrays were recorded following the B-band excitation. For the measurement of the B-band emission, the pump pulse was tuned to 405 nm to avoid interference from the scattered pump pulse near time zero. For the Q-band emission measurement, the excitation pulse was tuned to the B-band absorption maximum at 425 nm. The pump beam was focused to a 200-μm-thick cuvette containing sample solution by a 5-cm focal length lens. The cuvette was mounted on a motor-driven stage and moved constantly to minimize photodamage. Collection of the fluorescence and focusing it into a BBO crystal for the

(17) Shreve, A. P.; Trautman, J. K.; Frank, H. A.; Owens, T. G.; Albrecht, A. C. *Biochim. Biophys. Acta* **1991**, *1058*, 280.
(18) Joo, T.; Jia, Y.; Yu, J.-Y.; Jonas, D. M.; Fleming, G. R. *J. Phys. Chem.* **1996**, *100*, 2399.
(19) Chachisvilis, M.; Kühn, O.; Pullerits, T.; Sundström, V. *J. Phys. Chem. B* **1997**, *101*, 7275.
(20) Pullerits, T.; Chachisvilis, M.; Johnes, M. R.; Hunter, C. N.; Sundström, V. *Chem. Phys. Lett.* **1994**, *224*, 355.
(21) Jimenez, R.; Dikshit, S. N.; Bradforth, S. E.; Fleming, G. R. *J. Phys. Chem.* **1996**, *100*, 6825.
(22) Hess, S.; Feldchtein, F.; Babin, A.; Nurgaleev, I.; Pullerits, T.; Sergeev, A.; Sundström, V.; *Chem. Phys. Lett.* **1993**, *216*, 247.
(23) Hess, S.; Åkesson, E.; Cogdell, R. J.; Pullerits, T.; Sundström, V.; *Biophys. J.* **1995**, *69*, 2211.
(24) Martin, R. E.; Diederich, F. *Angew. Chem., Int. Ed. Engl.* **1999**, *38*, 1350.
(25) Osuka, A.; Tanabe, N.; Zhang, R. P. Maruyam, K. *Chem. Lett.* **1993**, 1505.
(26) Aratani, N.; Osuka, A.; Kim, Y. H.; Jeong, D. H.; Kim, D. *Angew. Chem., Int. Ed.* **2000**, *39*, 1458.
(27) Brodard, P.; Matzinger, S.; Vauthey, E.; Mongin, O.; Papamicael, C.; Gossauer, A. *J. Phys. Chem. A* **1999**, *103*, 5858.
(28) Biemans, H. A.; Rowan, A. E.; Verhoeven, A.; Vanoppen, P.; Latterini, L.; Foekema, J.; Schenning, A. P. H. J.; Meijer, E. W.; de Schryver, F. C.; Nolte, R. J. M. *J. Am. Chem. Soc.* **1998**, *120*, 11054.
(29) Schweitzer, G.; de Belder, G.; Latterini, L.; Karni, Y.; Rowan, A. E.; Nolte, R. J. M.; de Schryver, F. C. *Chem. Phys. Lett.* **1999**, *303*, 261.
(30) (a) Yeow, E. K. L.; Ghiggino, K. P.; Reek, J. N. H.; Crossley, M. J.; Bosman, A. W.; Schenning, A. P. H. J.; Meijer, E. W. *J. Phys. Chem. B* **2000**, *104*, 2596. (b) Choi, M.-S.; Aida, T.; Yamazaki, T.; Yamazaki, I. *Angew. Chem., Int. Ed.* **2001**, *40*, 3194. (c) Choi, M.-S.; Aida, T.; Yamazaki, T.; Yamazaki, I. *Chem. Eur. J.* **2002**, *8*, 2668.
(31) Yoon, M.-C.; Jeong, D. H.; Cho, S.; Kim, D.; Rhee, H.; Joo, T. *J. Chem. Phys.* **2003**, *118*, 164.

Scheme 1. Structures of the *o*-Dimer, *m*-Trimer, and Hexamer Optimized by Semiempirical PM3 Hamiltonian along with the Excitation Energy Hopping Process

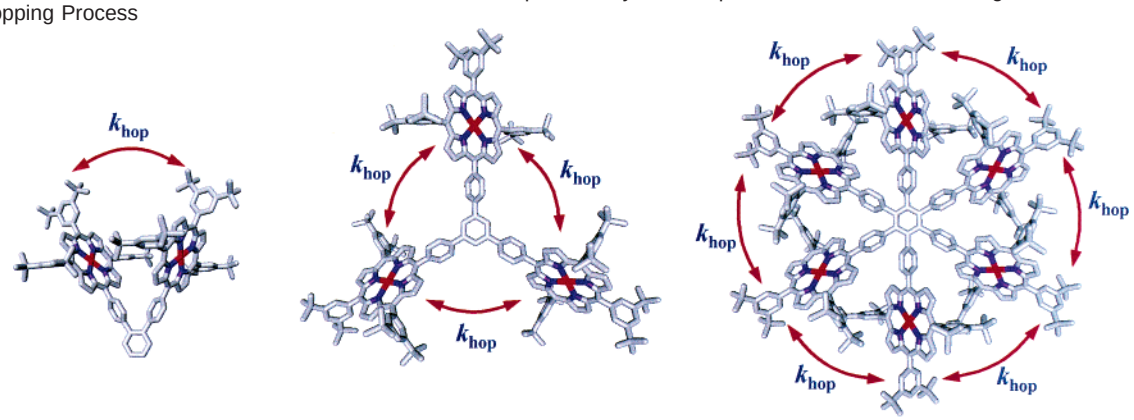

upconversion of fluorescence was achieved by a reflective microscope objective lens. A 100-μm-thick BBO crystal was used for the upconversion of the B-band emission, while a 500-μm-thick BBO crystal was used for the Q-band emission at the expense of time resolution. Their full width at half-maximums (fwhm) of the cross-correlation functions between the scattered pump pulse and the gate pulse were 70 and 150 fs, respectively.

For the anisotropy measurements, $I_{||}$ and $I_{\perp}$ were recorded to obtain the anisotropy, $r(t)$, and the rotation-independent fluorescence signal, $I_m(t)$

$$r(t) = (I_{||} - GI_{\perp})/(I_{||} + 2GI_{\perp}) \quad (1)$$

$$I_m(t) = I_{||} + 2GI_{\perp} \quad (2)$$

where $I_{||}$ and $I_{\perp}$ represent upconverted signals with the polarizations of the excitation and fluorescence being mutually parallel and perpendicular, respectively. The correction factor G was obtained by tail-matching fluorescences, $I_{||}$ and $I_{\perp}$, for a coumarin dye at long times.

To investigate the energy relaxation dynamics of the S_1 state in the absence of the excess energy effect, a time-correlated single photon counting (TCSPC) method was used with the photoexcitation of the Q-band. The picosecond excitation pulses at 580 nm were obtained from a cavity-dumped picosecond dye laser (Coherent 702) synchronously pumped by a mode-locked Nd:YAG laser (Coherent Antares). The cavity dumped beam from the dye laser has a 2-ps pulse width and an average power of ~30 mW at a 9.5-MHz dumping rate when rhodamine 6G was used as a gain dye. The emission was collected at a 90° angle with respect to the excitation laser beam by 5- and 25-cm focal length lenses, focused onto a monochromator (Jovin-Yvon HR320). The emission was detected with a thermoelectrically cooled MCP-PMT (Hamamatsu R3809U-51). The signal was amplified by a wide-band amplifier (Philip Scientific), sent to a Quad constant fraction discriminator (Tennelec), a time-to-amplitude converter (Tennelec), and a counter (Ortec), a multichannel analyzer (Tennelec/Nucleus), and stored in a computer. The excitation beam was vertically polarized, and the emission was obtained by using a combination of polarizer and depolarizer before the detection system. The instrumental response function was ~50 ps in fwhm.

1,3,5-Triphenylene-bridged triporphyrin (*m*-trimer) and 1,2-phenylene diporphyrin (*o*-dimer) were prepared by Suzuki coupling reaction of boronate Cu^{II}porphyrin with 1,3,5-tribromobenzene and 1,2-diiodobenzene followed by demetalation and zinc insertion.[32] Benzene-centered cyclic porphyrin hexamer (hexamer) was given by palladium- and cobalt-catalyzed trimerization of diphenylethynyl-bridged diporphyrin followed by demetalation with H_2SO_4 in trifluoroacetic acid to give free-base porphyrins and zinc insertion with $Zn(OAc)_2$ to afford Zn−porphyrins.[32] The samples were carefully characterized by the UV−visible spectroscopy, ^{1}H NMR spectroscopy, and MALDI-TOF mass spectrometry, which clearly demonstrate the high purity of the employed compounds.

The molecular structures of the *o*-dimer, *m*-trimer, and hexamer were obtained by the geometry optimization procedure, employing the semiempirical PM3 as well as AM1 Hamiltonian. The geometry of the porphyrin monomer was optimized, and our calculations have been focused mainly on the dihedral angle between the porphyrin rings. Both calculations show nearly identical results on the molecular structures of the *o*-dimer, *m*-trimer, and hexamer. The Förster energy-transfer rates could be estimated based on the calculated geometries.

Results

A. Steady-State Measurements. In the porphyrin array molecules employed in this study, each pair of porphyrin units is linked by triphenylene bridges (Scheme 1). Absorption spectra shown in Figure 1a clearly demonstrate weak couplings between porphyrin units in the Q state; the absorption spectra of Zn^{II}-TPP monomer, *o*-dimer, *m*-trimer, and hexamer in toluene are nearly identical, showing the 0−0 band at 590 nm and the dominant 0−1 band at 550 nm.

Interactions between porphyrin units in the B state are stronger than those in the Q state because of the much larger transition dipole moment. The Soret band of the *o*-dimer is split into two bands, appearing significantly broader than those of other porphyrin arrays. Both transitions of the split bands should be allowed, since the relative angle between the transition dipoles of the *o*-dimer is ~60°. The absorption band may be deconvoluted by the two Gaussian functions centered at 421 and 429 nm, indicating that the B states in the *o*-dimer interact strongly due to a shorter distance between the two porphyrin units. On the other hand, the B-band of the *m*-trimer is the most red-shifted and that of the hexamer is located between those of the *o*-dimer and *m*-trimer. According to the exciton coupling theory,[33,34] the high-lying degenerate excitonic transitions are allowed in the *m*-trimer, whereas the lowest degenerate transitions are allowed in the hexamer (Figure 2). The B-band of the hexamer is broader and slightly red-shifted compared to the monomer, although the distances between the neighboring porphyrin units in the *o*-dimer and hexamer may be regarded to be nearly the same.

(32) Takase, M.; Ismael, R.; Murakami, R.; Ikeda, M.; Kim, D.; Shinmori, H.; Furuta, H.; Osuka, A. *Tetrahedron Lett.* **2002**, *43*, 5157.

(33) Kasha, M.; Rawls, H. R.; El-Bayoumi, M. A. *Pure Appl. Chem.* **1965**, *11*, 371.

(34) Van Oijen, A. M.; Ketelaars, M.; Köhler, J.; Aartsma, T. J.; Schmidt, J. *Science* **1999**, *285*, 400.

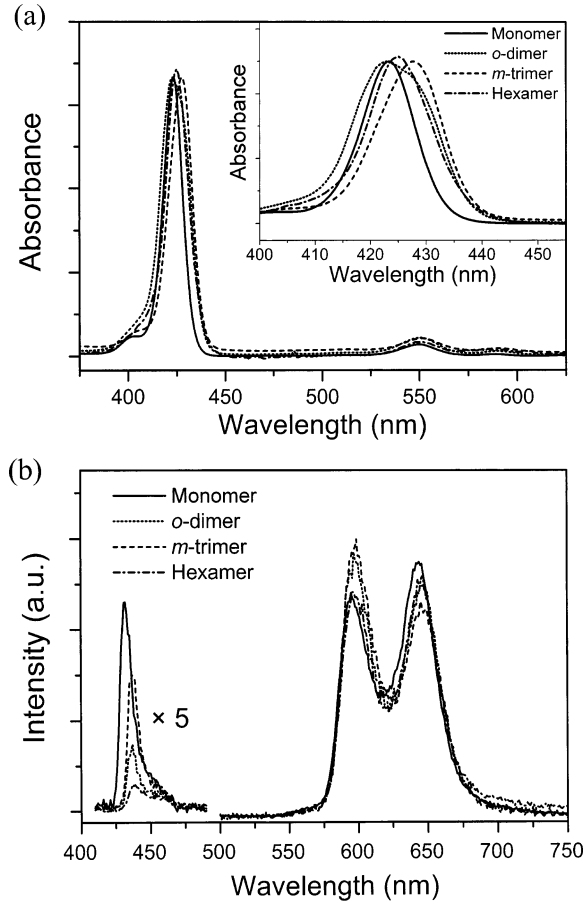

Figure 1. (a) Steady-state absorption and (b) emission spectra of the monomer (solid), *o*-dimer (short dot), *m*-trimer (dot), and hexamer (dash dot). Inset of (a) shows Soret absorption region. The Q-band emissions are normalized by the integrated total emission intensity, and the B-band emissions are magnified 5 times.

The geometry optimization by using the PM3 Hamiltonian shows that the porphyrin moiety in these arrays gives rise to the dihedral angle of ∼85° with the linked phenyl group (Scheme 1). The dihedral angles between the adjacent phenyl group and the central benzene unit are ∼47, ∼51, and ∼57° in the *m*-trimer, *o*-dimer, and hexamer, respectively. Therefore, π-conjugation is expected to be slightly larger in the *m*-trimer than in the hexamer. In this regard, the most red-shifted B-band of the *m*-trimer can be explained by the π-conjugation between porphyrin units and benzene rings despite the weakest interunit interactions among the arrays. In addition, much smaller steric hindrance between porphyrin moieties due to large inter-porphyrin distance can enhance the stabilization of the B states in the *m*-trimer, which is also responsible for the most red-shifted absorption band.

The steady-state B- and Q-band emissions are shown in Figure 1b. The Q-band emissions show the spectral features observed in typical Zn^{II}porphyrins; two bands at 600 and 645 nm, which are assigned to 0−0 and 1−0 vibronic transitions. All emission spectra were normalized according to the integrated intensity of Q-band emission. As shown in Figure 1b, the stationary B-band emissions can be measured readily owing to relatively long S_2 state lifetimes and the B-band emission intensities decrease in order of the monomer, *m*-trimer, *o*-dimer, and hexamer. Since the Q-band emission lifetimes of all four molecules are nearly identical to ∼2 ns and the Q-band

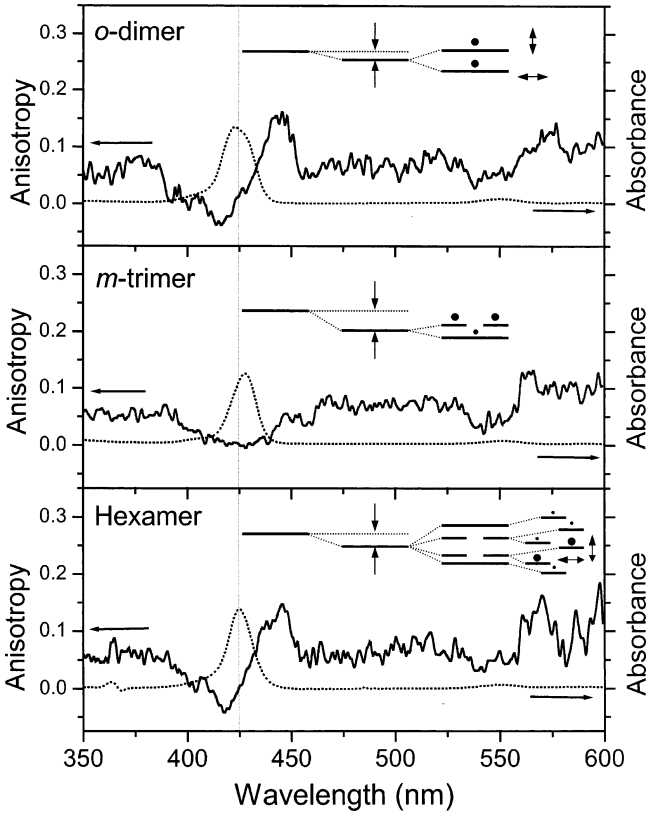

Figure 2. Stationary fluorescence excitation anisotropy spectra of the *o*-dimer (top), *m*-trimer, and hexamer (bottom). The insets suggest the electronic states induced by exciton coupling and their dipoles' orientation. See the text for the details.

Table 1. Stationary Spectroscopic Data of the Porphyrins

	B-band			Q-band	
	λ_{abs} (nm)	$\Delta\omega_{abs}$ (cm^{-1})[a]	λ_{em} (nm)	λ_{Abs} (nm)	λ_{em} (nm)
monomer	423	640	432 (1.0)[b]	549, 589	596, 644
o-dimer	424 (421, 429)[c]	960	437 (0.32)	550, 590	598, 646
m-trimer	427	750	437 (0.63)	550, 590	598, 646
hexamer	425	750	437 (0.15)	550, 590	598, 646

[a] Full width at half-maximum of the Soret absorption band. [b] Numbers in parentheses represent the relative intensities of the B-band emission.[c] Peak positions when fitted by two Gaussian functions.

extinction coefficients are also nearly the same, the Q-band fluorescence quantum yields may be assumed to be the same. Therefore, the intensities of B-band emissions normalized to the Q-band emission correspond to the relative fluorescence quantum yields of the B-band emissions, which imply the rates of the B → Q internal conversion. The lifetimes obtained from the B-band emission intensities are consistent mostly with those measured directly by TRF measurement that will be described below. All the stationary spectroscopic data are summarized in Table 1.

To obtain information on the relative orientation between the absorption and emission dipoles of the porphyrin arrays, the fluorescence excitation anisotropy spectra were measured (Figure 2). The anisotropy spectra show that the relative orientations between the transition dipoles of the B and Q states are slightly different in *o*-dimer, *m*-trimer, and hexamer. It is noteworthy that the fluorescence excitation anisotropy spectra

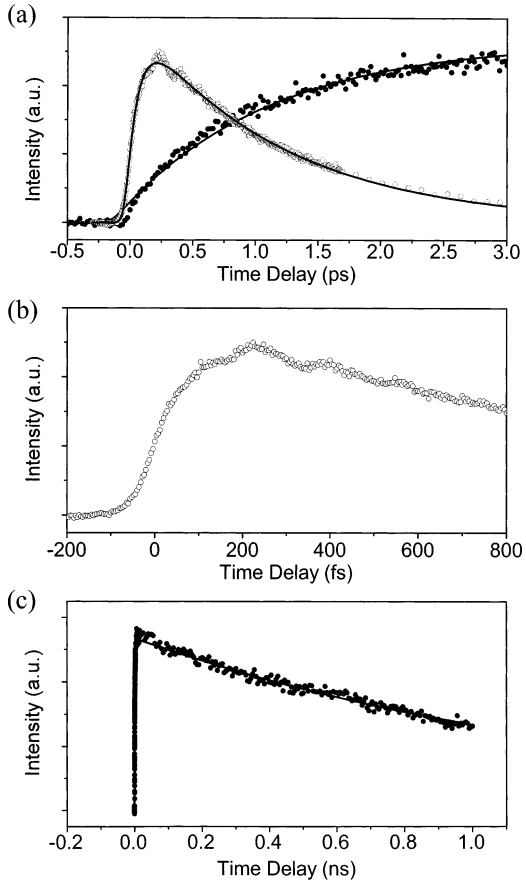

Figure 3. Fluorescence temporal profiles of the monomer after photoexcitation at 405 nm. (a) B-band decay (open circle) and Q-band (650 nm) rise (filled circle). (b) Oscillations of B-band emission in the short time window. (c) Q-band decay in the long time window. See Table 2 for the details.

of the *o*-dimer and hexamer are similar to each other while that of the *m*-trimer shows spectral features close to the Zn^{II}porphyrin monomer,[35] being consistent with the fact that the B-band of the *m*-trimer arises from the transition to the degenerate states (Figure 2). The B-band anisotropy spectra of the *o*-dimer and hexamer exhibit a differential form of the absorption spectra with a slight phase shift. This indicates that the origin of the red and blue side of the B-band is different. In the *o*-dimer, the directions of the two transition dipoles may be considered to be orthogonal to each other as shown in Figure 2. In the hexamer, the first degenerate states are expected to be coupled to the lowest state due to static or dynamic disorder to produce two bands, which gives rise to a typical anisotropy spectrum of the hexamer as shown in Figure 2.

B. Time-Resolved Fluorescence of the Monomer. Figure 3 shows time-resolved spontaneous emission of Zn^{II}TPP in toluene following excitation at 405 nm. The B- and Q-band emissions were detected at 440 and 650 nm, respectively. The B state of Zn^{II}TPP shows relatively strong emission, a rare exception of the Kasha rule. Owing to its relatively long lifetime, the time-resolved emission of the B state has been reported previously by several groups.[36−39] In addition, the probe wavelength dependence of the fluorescence decay profiles of the monomer has also been studied. The detection wavelength

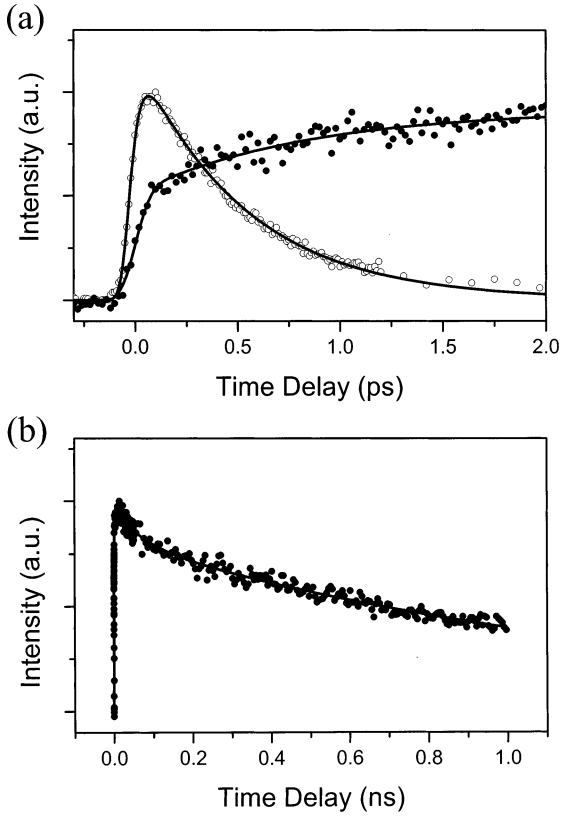

Figure 4. Fluorescence temporal profiles of the *o*-dimer after photoexcitation at 425 nm. (a) B-band decay (open circle) and Q-band (650 nm) rise (filled circle). (b) Biexponential decay of Q-band. See Table 2 for the details.

dependence was explained in terms of the emission from the vibrationally excited S_1 state, which was rapidly populated from the upper states, in addition to the emission from the vibrational ground S_1 state. The temporal profile of the B state emission shows an initial rise and a subsequent decay with time constants of 90 fs and 1.2 ps, respectively. The rise component may be assigned to the spectral relaxation caused by solvation and vibronic relaxation processes, while the 1.2-ps decay is due to the B → Q internal conversion. The signal also shows oscillations at 202 and 383 cm^{-1} due to the wave packet motion in the B state, which demonstrates a high time resolution of the current measurement. The TRF of the Q-band emission shows a single-exponential rise of 1.2 ps. The excellent agreement between the B-band decay and the Q-band rise time constants confirms that the 1.2-ps component is due to the B → Q internal conversion process.

C. Time-Resolved Fluorescence of the Porphyrin Arrays. As indicated by the absorption spectrum, a close proximity between the porphyrin units in the *o*-dimer causes significant through-space interactions in the B states. The strong interactions between porphyrin units have been reported to lead to faster B → Q internal conversion rates. From the intensity of the stationary fluorescence, the B state lifetime of the *o*-dimer is estimated to be ∼400 fs, which is shorter than that of the monomer (1.2 ps).

(35) Kim, Y. H.; Jeong, D. H.; Kim, D.; Jeoung, S. C.; Cho, H. S.; Kim, S. K.; Aratani, N.; Osuka, A. *J. Am. Chem. Soc.* **2001**, *123*, 76.
(36) Song, N. W.; Cho, H. S.; Yoon, M.-C.; Jeoung, S. C.; Yoshida, N.; Osuka, A.; Kim, D. *Bull. Chem. Soc. Jpn.* **2002**, *75*, 1023.
(37) Mataga, N.; Shibata, Y.; Chosrowjan, H.; Yoshida, N.; Osuka, A. *J. Phys. Chem. B* **2000**, *104*, 4001.
(38) Akimoto, S.; Yamazaki, T.; Yamazaki, I.; Osuka, A. *Chem. Phys. Lett.* **1999**, *309*, 177.
(39) Yu, H.-Z.; Baskin, S.; Zewail, A. H. *J. Phys. Chem. A* **2002**, *106*, 9845.

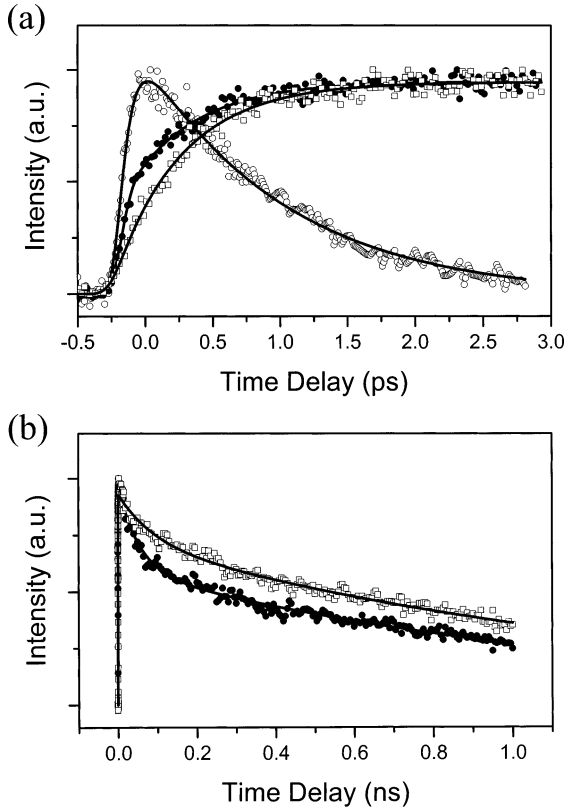

Figure 5. Fluorescence temporal profiles of the *m*-trimer after photoexcitation at 425 nm. (a) B-band decay (open circle) and Q-band rises at 600 (filled circle) and 650 nm (open square). (b) Q-band decays in the long time window. See Table 2 for the details.

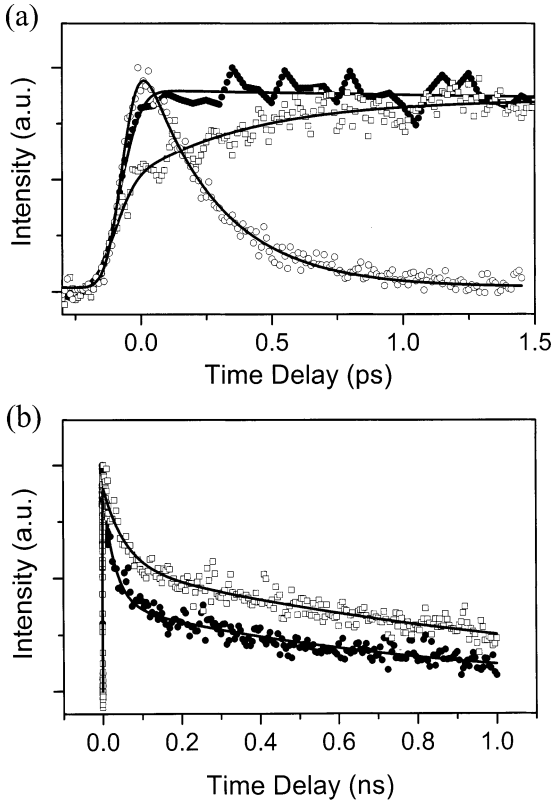

Figure 6. Fluorescence temporal profiles of the hexamer after photoexcitation at 425 nm. (a) B-band decay (open circle) and Q-band rises at 600 (filled circle) and 650 nm (open square). (b) Q-band decays in the long time window. See Table 2 for the details.

TRF decays of the *o*-dimer in toluene following B-band excitation are shown in Figure 4. The B-band emission shows a single-exponential decay with a time constant of 520 fs, in good agreement with the value estimated from the intensity of the spontaneous emission (~400 fs). Temporal profiles of the Q-band emission, however, display rather complicated behavior. The emission detected at 650 nm consists of two components: an ultrafast instrument-limited rise and a slower rise component with a time constant of ~710 fs. The difference between the B-band decay and the slower rise time constant is beyond the experimental uncertainty. Moreover, the Q-band emission at 650 nm shows an ~85-ps decay component in addition to the slow Q state population relaxation of a long time constant (~1.8 ns).

TRF following B-band excitation for the *m*-trimer and hexamer in toluene are shown in Figures 5 and 6, respectively. The B-band decay time constant of the *m*-trimer is ~980 fs, which is comparable to the value estimated from the B-band fluorescence intensity (~800 fs). The similarity between the internal conversion rates in the monomer and *m*-trimer indicates that interactions between the porphyrin units in the *m*-trimer are weaker than those in the *o*-dimer. The B-band decay time constant of the hexamer is 310 fs, which is also comparable to the value estimated from the B-band emission intensity (~200 fs). Increase of the internal conversion rate in order of the monomer, *m*-trimer, *o*-dimer, and hexamer demonstrates clearly that the internal conversion rate is related closely to the electronic interactions in the Soret states; that is, the increase of the density of states induced by the intermolecular excitonic interactions gives rise to stronger couplings between the S_2 and S_1 states in the porphyrin arrays, hence enhancing the internal conversion rates.

Time-resolved emission profiles of the Q-band in the *m*-trimer and hexamer exhibit qualitatively the same behavior as observed in the *o*-dimer. The Q-band emission of the *m*-trimer at 650 nm shows a small-amplitude instrument-limited ultrafast rise and a 540-fs rise. It is noteworthy that the rise time constant of the Q-band emission is faster than the decay time constant of the B-band emission. In the hexamer, the Q-band emission at 600 nm is dominated by an instrument-limited rise, while the signal shows an instrument-limited ultrafast rise and a 530-fs rise at 650 nm. For the hexamer, the rise time of the Q-band emission does not coincide with the decay time of the B-band emission. The rise and decay time constants for all the porphyrin arrays are summarized in Table 2.

D. Time-Resolved Fluorescence Anisotropy. TRF anisotropy measurement can give detailed information on the dynamics of intermolecular and intramolecular EET processes. When an initial excitation is transferred to a state whose transition dipole moment is different in direction from that of the initial state, the anisotropy decays according to the transfer rate. Especially, the time-resolved anisotropy measurement in a multichromophore system is useful in studying the EET processes. For the array systems under scrutiny, TRF anisotropy is expected to provide useful information on the B ↔ B and Q ↔ Q electronic excitation transfer, which is otherwise difficult to obtain.

Until now, there have been simple theoretical models that treat a multichromophore system regarding the depolarization process. A key difference in these models is whether they treat

Table 2. Time Constants from Nonlinear Least Square Fits of the Time Resolved B Band Emission at 442 nm and Q Band Emission at 600 and 650 nm

	B-band	Q-band			
	$\lambda_{det} = 442$ nm	$\lambda_{det} = 600$ nm		$\lambda_{det} = 650$ nm	
		rise	decay	rise	decay
monomer	1.2 ps	1.2 ps	long[a]	1.2 ps	long
o-dimer	520 fs	ultrafast	25 ps long	ultrafast[b] 710	85 ps long
m-trimer	980 fs	ultrafast	55 ps long	ultrafast 540 fs	80 ps long
hexamer	310 fs	ultrafast	30 ps long	ultrafast 530 fs	50 ps long

[a] Represents a long decay component, which may be more accurate in the TCSPC measurement than in the fluorescence upconversion one and is ~2.5 ns. After photoexcitation of the S_1 state at 580 nm, the long-lived fluorescence component of the hexamer was observed to decay with a lifetime of ~2.5 ns in toluene. The fluorescence lifetimes of the *o*-dimer (~1.8 ns) were observed to be similar to that of the *m*-trimer in toluene. [b] Represents a faster rise component than our time resolution.

the transition dipoles of the molecular system as randomly oriented or well-defined. Assuming that the intermolecular interactions are weak, the excitation energy hopping dynamics in the hexamer can be approximately described by Scheme 1, in which k_{hop} is the excitation energy hopping rate. The excitation energy hopping process is assumed to occur only between adjacent porphyrin units. When a porphyrin is photoexcited, time evolution of the excitation energy population in each chromophore will be given by the following equation.

$$d\mathbf{P}/dt = \mathbf{KP} \tag{3}$$

where **P** is the excitation energy population vector and **K** is the rate coefficient. For the hexamer, **K** is expressed by a 6 × 6 matrix,

$$\mathbf{K} = \begin{bmatrix} -(k_F + 2k_{hop}) & k_{hop} & 0 & 0 & 0 & k_{hop} \\ k_{hop} & -(k_F + 2k_{hop}) & k_{hop} & 0 & 0 & 0 \\ 0 & k_{hop} & -(k_F + 2k_{hop}) & k_{hop} & 0 & 0 \\ 0 & 0 & k_{hop} & -(k_F + 2k_{hop}) & k_{hop} & 0 \\ 0 & 0 & 0 & k_{hop} & -(k_F + 2k_{hop}) & k_{hop} \\ k_{hop} & 0 & 0 & 0 & k_{hop} & -(k_F + 2k_{hop}) \end{bmatrix} \tag{4}$$

where the k_F represents the fluorescence decay rate of an individual porphyrin chromophore. Assuming that the transition dipoles are randomly oriented, the fluorescence anisotropy decay dynamics of the *m*-trimer and hexamer are described by the following equations.

$$r(t) = r_0\left\{\frac{1}{3} + 0.666e^{-3k_{hop}t}\right\} \quad \text{for the trimer} \tag{5}$$

$$r(t) = r_0\left\{\frac{1}{6} + 0.33e^{-k_{hop}t} + 0.33e^{-3k_{hop}t} + 0.17e^{-4k_{hop}t}\right\} \quad \text{for the hexamer} \tag{6}$$

Anisotropy decay due to rotational diffusion is ignored in the above equation, since the time scale of the process is a few hundred picoseconds.

One thing to be considered here is that the degeneracy of the B (and Q) state of the porphyrin monomer complicates the anisotropy decay analysis considerably. Electronic dephasing and the intramolecular energy equilibration between the degenerate B_x and B_y states can occur prior to the EET process between Zn^{II}porphyrin moieties. For a degenerate system with their transition dipole moments mutually orthogonal, as in the B state of a porphyrin with D_{4h} symmetry such as Zn^{II}TPP, Wynne and Hochstrasser showed that time-dependent anisotropy $r(t)$ is given by[40,41]

$$r(t) = \frac{1}{10}\{1 + 3e^{-\gamma t} + 3f(t)\} \tag{7}$$

$$f(t) = \left[\frac{\gamma/2 - \Gamma}{\Omega}\sin(\Omega t) + \cos(\Omega t)\right]e^{-((\gamma/2)+\Gamma)t} \tag{8}$$

where γ represents an electronic coherence decay caused by the energy fluctuations and Γ is a decay associated with the coupling fluctuations between the two states. According to this equation, the anisotropy shows an initial value of 0.7, larger than the normally observed value 0.4, before electronic dephasing sets in. After the two states are completely dephased with equal population, the anisotropy attains a value of 0.1.

As mentioned above, the B ↔ B (Q ↔ Q) energy-transfer processes among porphyrin moieties will further reduce the anisotropy value for the *m*-trimer and hexamer, whereas the asymptotic value for the *o*-dimer depends on the angle between the porphyrin units. The semiempirical calculation by the PM3 Hamiltonian indicates that the hexamer is star-shaped with tilted facial structure to make an angle of 60° from the horizontal plane rather than a meridional one between the two neighboring Zn^{II}porphyrins. Thus, six degenerate transition dipoles of the hexamer can be considered to reside roughly on the radial direction to the hexagonal plane, while the other six are on the perpendicular direction, which do not have an effect on the depolarization process caused by the intermolecular EET process when the rotational diffusion is ignored. The slightly tilted structures of our porphyrin arrays, however, could induce the depolarization process for the dipoles on the perpendicular directions, which may be considered to be negligible. As a result, only the radial direction transition dipoles of the hexamer should be considered after the initial ultrafast depolarization within each porphyrin unit, which occurs in ~100 fs caused by the electronic dephasing and population equilibration. For a ring structure without disorder, the analytical depolarization time was obtained by Leegwater.[42]

$$\tau_{dep} = \frac{\tau_{hop}}{4\sin^2(2\pi/N)} \quad \text{for a small interaction} \tag{9}$$

For the *m*-trimer and hexamer, the depolarization time is calculated to be ~3 times slower than the hopping time. This

(40) Wynne, K.; Hochstrasser, R. M. *Chem. Phys.* **1993**, *171*, 179.
(41) Wynne, K.; Hochstrasser, R. M. *J. Raman Spectrosc.* **1995**, *26*, 561.
(42) Leegwater, J. A. *J. Phys. Chem.* **1996**, *100*, 14403.

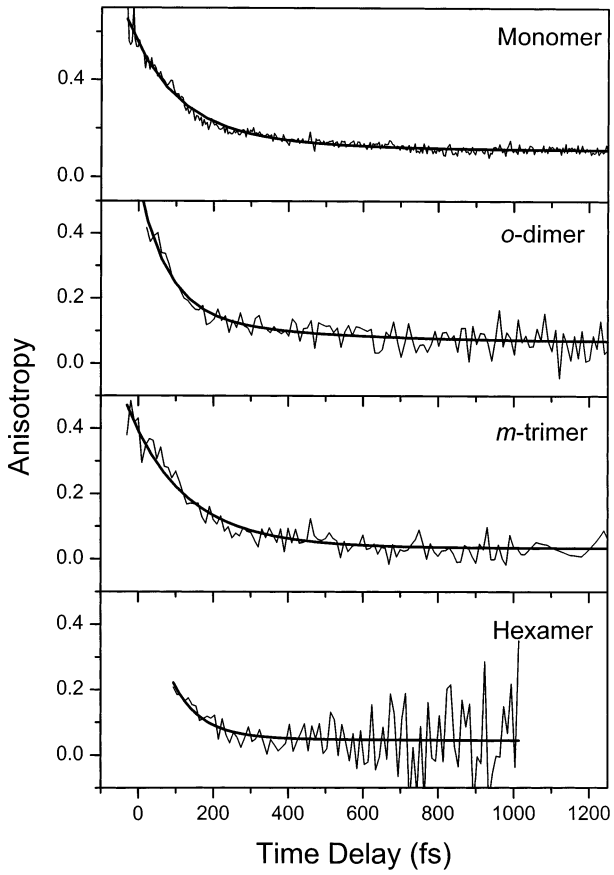

Figure 7. Anisotropy decay profiles of the B-band emission following 405-nm photoexcitation of the monomer, *o*-dimer, *m*-trimer, and hexamer from top to bottom. See Table 3 for the details.

indicates that depolarization by the intermolecular EET can be described by a single-expoential function. It is interesting to note that the same depolarization rate constant ($3k_{hop}$) is predominant even in the case where the transition dipoles of the *m*-trimer and hexamer are randomized (eqs 5 and 6). Based on this background, the time-resolved anisotropy data shown in Figure 7 were analyzed and the hopping rates were estimated, which reveals that the fluorescence anisotropy decay is not a single exponential. The anisotropy decay profile of the monomer can be fitted adequately by a biexponential function as eqs 7 and 8 predict. According to the biexponential fit, the anisotropy starts from 0.7 and decreases by the time constants of 75 and 380 fs to an asymptotic value of 0.11. The initial and final anisotropy values of the monomer match well with the theoretical consideration.

For the arrays, the anisotropy decay arises from the inter-porphyrin EET as well as the electronic dephasing between B_x and B_y dipoles of the monomer unit. The anisotropy decays of the *m*-trimer and hexamer can be expressed by three components: $\tau_{mono}^{(1)}$, $\tau_{mono}^{(2)}$, and $\tau_{hop}/3$. Thus, the overall decay profiles were fitted by a biexponential function obtained from the monomer and an exponential function that represents the EET in the arrays. The estimated hopping rates of the porphyrin arrays are listed in Table 3. The hopping times between the porphyrin units in the *o*-dimer and hexamer were estimated to be ~100 and ~220 fs and that in the *m*-trimer was ~450 fs, although it has an uncertainty due to the small difference in the anisotropy decay profile between the monomer and *m*-trimer.

Table 3. Fitting Results for the Anisotropy Decay, $r(t)$, and Estimated Hopping Time

sample		time constant	$r(\infty)$	τ_{ET}[a]	$\tau_{ET}^{Förster}$ [b]
monomer		75, 380 fs[c]	0.11		
o-dimer	B-band	100 fs[d]	0.08	100 fs	172 fs
	Q-band	60 ps (580 ps)[e]		60 ps	78 ps
m-trimer	B-band	150 fs[d]	0.04	450 fs	6.7 ps
	Q-band	90 ps (800 ps)[e]		270 ps	3.1 ns
hexamer	B-band	73 fs[d]	0.04	220 fs (125 fs)[f]	246 fs
	Q-band	60 ps (2.8 ns)[e]		180 ps (130 ps)[f]	111 ps

[a] The energy-transfer times in *m*-trimer and hexamer were obtained by 3 times the anisotropy decay times. [b] The time constants were calculated based on the Förster equation. See the text for the details. [c] The time constants from a biexponential fit. [d] The time constants in the B states of *o*-dimer, *m*-trimer, and hexamer were obtained by the function, in the form of $A_1 r_m(t) + A_2 \exp(-t/\tau)$. Only the τ values excluding monomer anisotropy decay are shown here (see text for details). [e] The values in parentheses are second-exponential time constants, which are assigned to the rotational diffusion processes. [f] These time constants were obtained when fitted by eq 6 in the text.

Based on eq 6, the hopping time of the hexamer was determined to be ~125 fs, which is close to the value (220 fs) obtained from eq 9, despite the different treatment of the transition dipoles (randomly oriented vs well-defined).

Assuming that there is no preferred mutual orientation between porphyrin moieties, the residual anisotropy value is inversely proportional to the number of chromophores according to the Master equation (3). Accordingly, the porphyrin array systems show that the residual anisotropy value has a tendency to decrease as the number of porphyrin units increases from the *o*-dimer to hexamer, though the residual anisotropy value does not exactly follow such a simple model. This indicates that porphyrin molecules retain complicated three-dimensional structures to some degree and that there are static and dynamic disorders at room temperature, especially in the distributions of dihedral angle between porphyrins and phenyl groups including the central benzene.

Figure 8 shows slow anisotropy decay profiles of the *o*-dimer, *m*-trimer, and hexamer after photoexcitation of the Q state. The anisotropy decays were fitted by two exponential functions, where the fast component is considered to arise from the EET between porphyrin moieties in the Q state and the slow component is due to the rotational diffusion dynamics. The energy-transfer rates, thus, were obtained to be ~60, ~270, and ~180 ps, for the *o*-dimer, *m*-trimer, and hexamer in a manner similar to the cases of the B state energy transfer. When the anisotropy decay profile of the hexamer was fitted by eq 6, the excitation energy hopping time was estimated to be ~130 ps, also close to the value obtained by the single-exponential anisotropy decay. The rotational diffusion times (τ_{rot}) for the porphyrin monomer, *o*-dimer, *m*-trimer, and hexamer were observed to be 170 ps, 580 ps, 800 ps, and 2.8 ns, respectively. The rotational diffusion time is given by the Stokes−Einstein−Debye relation as follows.

$$\tau_{rot} = V\eta/kT \qquad (10)$$

where τ_{rot} is the rotational diffusion time obtained by using the hydrodynamic volume V, solvent viscosity η, Boltzman constant k, and temperature T. Thus, the estimated large hydrodynamic volume of the hexamer is in a good agreement with the much slower rotational diffusion time as compared with the other porphyrin arrays.

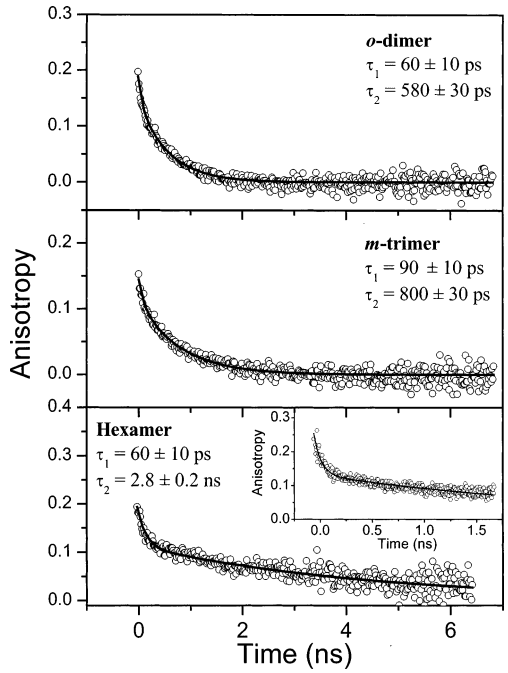

Figure 8. Anisotropy decay profiles of the Q-band emission following 580-nm photoexcitation of the *o*-dimer, *m*-trimer, and hexamer from top to bottom. See Table 3 for the details.

Discussion

For the porphyrin arrays attached by a short linker or linked directly, the interactions between the B states are large enough to show well-separated exciton bands, whereas much weaker interactions are observed between the Q states. For example, coupling strengths between the B states and between the Q states in meso−meso directly coupled porphyrin wires were obtained to be about 2150 and 135 cm^{-1}, respectively.[35] For the porphyrin arrays studied here, the absorption spectra indicate that perturbations in the Q-bands are negligible, while weak perturbations are observed in the B-bands. The B-band absorption line widths of the *m*-trimer and hexamer increase roughly by the same amount (17%) from that of the monomer, while the absorption line width is significantly broader in the *o*-dimer.

Intermolecular interactions may be categorized into through-bond (Dexter-type) and through-space (Förster-type) interactions.[43,44] In our previous study on the energy-transfer processes in various Zn(II)- and free-base porphyrin systems,[45] it was observed that the energy-transfer mechanism even in porphyrin donor/acceptor systems bridged with long linkers were explained by through-bond as well as through-space interactions. Therefore, the two intermolecular interactions will be considered in discussing the electronic properties induced by the interporphyrinic coupling in the present porphyrin array systems in order to gain clear insight into porphyrin array systems.

TRF data including internal conversion rates and anisotropy decays show consistently that the dynamics are governed by through-space interactions in these porphyrin array systems. The *o*-dimer and hexamer, where the contribution by through-space interactions are much stronger than that by through-bond interactions because of the shorter inter-porphyrin distances, show faster dynamics than the *m*-trimer. On the other hand, the overall characteristics of the *m*-trimer are similar to the monomer due to larger inter-porphyrin distances, although through-bond interactions arising from π-conjugation should be considered to explain the photophysical properties. In the *m*-trimer, through-bond interactions are expected to be stronger than through-space ones judging from the time-resolved emission as well as the steady-state absorption/emission spectra.

The anisotropy decay rates of the arrays can be qualitatively well described by the sum of the energy hopping rates between porphyrin moieties and a considerable portion of dephasing/depopulation rates within the monomer, which indicates that the electronic excitation energy is localized initially on one porphyrin unit. At present, the porphyrin array systems studied here are assumed to belong to the weak interaction regime from the steady-state and time-resolved spectroscopic data, and the EET processes will be described by the incoherent hopping processes between the neighboring porphyrins.

The temporal profiles of the Q-band emissions exhibit detection wavelength dependences, that is, spectral dynamics of the emission, and the Q-band emission is composed of the two rise components, i.e., an instantaneous rise and a subsequent slower one. They are inconsistent with the decay profiles of the B-band emissions, which decay mainly with a single-exponential component. To explain the emission wavelength dependences of the porphyrin arrays including the monomer, three possibilities may be considered: (1) dynamic Stokes shift due to solvation processes as commonly observed in many dipolar solution systems; (2) intramolecular vibrational redistribution (IVR) and vibronic relaxation process after the B → Q internal conversion; (3) a third state overlapped with the B-band and coupled strongly with the Q state. First, the observed absorption and emission spectra indicate that the Stokes shift is quite small, and thus, this cannot account for the detection wavelength dependence.

Second, the spectral dynamics can be adequately accounted for by invoking IVR and vibronic relaxation within the Q state if IVR and vibronic relaxation occur much faster than the B → Q internal conversion rate. The detection wavelength dependences have been reported for Zn^{II}porphyrin monomers by several groups. Mataga et al. have observed kinetics depending on the detection wavelength in the TRF of Zn^{II}DPP in THF.[37] They explained the wavelength-dependent dynamics by the internal conversion and fast vibrational energy relaxation processes. In another TRF of DPP−OEP (diphenyl- and octaethyl-substituted)-type Zn^{II}porphyrin by Yamazaki et al.,[38] the energy relaxation from a vibrationally excited state around at 560 nm to a lower excited state in the Q state on a time scale of 600 fs was observed. The dependence of Q-band emission on the detection wavelength implies spectral dynamics in the TRF spectra; that is, the emission spectra shift to longer wavelengths as time goes on.

However, a decay or rise component with a few tens of picosecond usually observed in the porphyrin monomer due to vibrational cooling processes could not be explained by the fast vibrational energy relaxation model. Therefore, Zewail and coworkers have proposed a third state lying close to the B state but displaying different photophysical characteristics to account for their TRF and transient absorption spectra of Zn^{II}TPP.[39]

(43) Förster, T. *Discuss. Faraday Soc.* **1959**, *27*, 7.
(44) Dexter, D. L. *J. Chem. Phys.* **1953**, *21*, 836.
(45) Cho, H. S.; Jeong, D. H.; Yoon, M.-C.; Kim, Y. H.; Kim, R.-Y.; Kim, D.; Jeoung, S. C.; Kim, S. K.; Aratani, N.; Shinmori, H.; Osuka, A. *J. Phys. Chem. A* **2001**, *105*, 4200.

Scheme 2. Energy Relaxation Dynamics Scheme in the Porphyrin Arrays Following the B-Band Excitation[a]

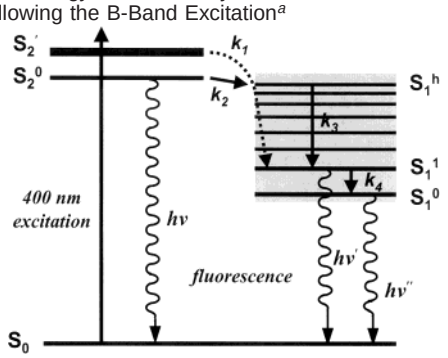

[a] It is assumed that there exists an S_2' state near the S_2 state and strong coupling (k_1) between the S_2' and S_1^1 for a reasonable explanation of the energy relaxation dynamics. The k_2 and k_3 exhibit internal conversion (IC) from the S_2 to S_1 state and the vibrational relaxation processes, respectively. See the text for the details.

Since the observed instrument-limited rise and a few tens of picosecond component observed in the Q state cannot be described clearly by the fast vibrational relaxation model, the fluorescence dynamics near the Q-band region can be explained more plausibly by the model proposed by the Zewail group. In our experiment, the rise component with a few hundred femtoseconds becomes more apparent in the porphyrin arrays such as *the o*-dimer and hexamer, and a little longer component of 50−85 ps was observed as a decay component instead of the well-known vibrational cooling process (∼20 ps). The reason for the absence of the ∼20-ps component is that it may be hidden in this large slow component due to its relatively small amplitude. It is to be noted that the slow component was observed in the porphyrin arrays but not in the porphyrin monomer. Thus, although the origin of the 50−85-ps component is still ambiguous, this component may be related to the energy transfer or conformational dynamics in the porphyrin arrays.

Accordingly, the fluorescence dynamics occurring early can be described by the energy relaxation model as depicted in Scheme 2 with some assumptions to simulate the kinetic model: (1) The fluorescence at 430 nm originates mainly from the S_2^0 state. The k_2 values were assumed to be 0.5, 0.9, and 0.3 ps^{-1} in the *o*-dimer, *m*-trimer, and hexamer, respectively, on the basis of the observed fluorescence decay rates. (2) Assuming that a higher lying S_2' state is strongly coupled to the S_1 state, playing a key role in the energy relaxation dynamics, the population after photoexcitation around at the S_2' state flows down very fast to near the bottom of the S_1 state. The k_1 values are assumed to be large due to the strong coupling to the S_1 state, of which values are 0.1, 0.2, and 0.1 ps^{-1} in the *o*-dimer, *m*-trimer, and hexamer, respectively. (3) The k_3 rate constant of 20 ps^{-1} originates from the vibrational cooling processes, which should not be omitted for the overall view of energy relaxation dynamics. (4) The vibrational relaxation from the S_1^1 to S_1^0 is assumed to be fast based on the observation that the fluorescence from the Q-band exhibits the instrument-limited rise after photoexcitation at 550 nm by a femtosecond upconversion experiment, so that the rate constant k_4 is assumed to be 0.2 ps^{-1}. The subsequent kinetic simulations of the *o*-dimer, *m*-trimer, and hexamer are shown in Figure 9, and they are in a good agreement with the observed fluorescence temporal profiles.

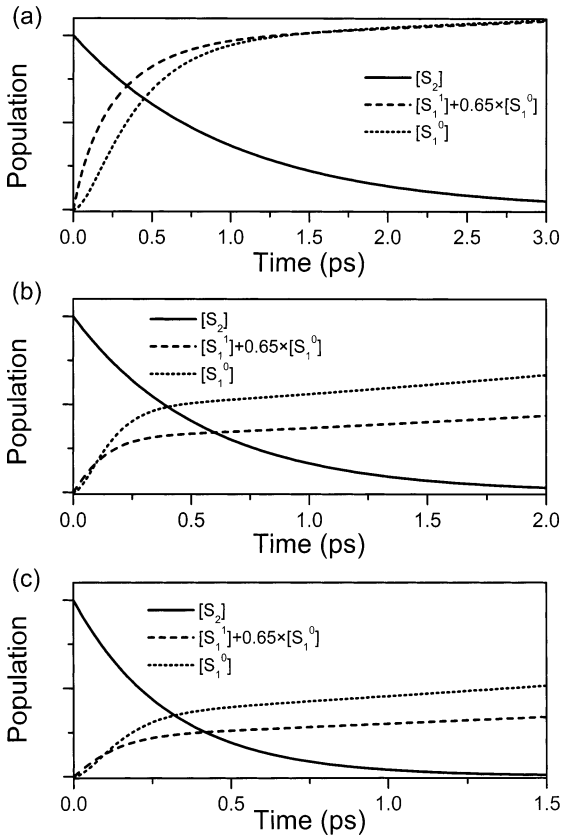

Figure 9. Population decay dynamics of (a) *o*-dimer, (b) *m*-trimer, and (c) hexamer simulated on the basis of the Scheme 2. These simulations were compared and matched well with the observed fluorescence profiles. For details of the kinetic constants (k_1, k_2, k_3, k_4), refer to the text.

To gain further insight into the excitation energy hopping processes occurring in the porphyrin arrays, we have calculated the energy-transfer rate of the *o*-dimer, *m*-trimer, and hexamer in the B and Q states by using the Förster equation as follows.[43]

$$k = \frac{8.8 \times 10^{-25}\kappa^2}{n^4 R^6 \tau} J' \tag{11}$$

$$J' = \int F(\nu)\epsilon(\nu)n^{-4}\,\mathrm{d}\nu \tag{12}$$

where n is the refractive index of the solvent, R is the center-to-center distance between the energy donor and acceptor, τ is the fluorescence lifetime of the energy donor, κ is the dipole−dipole orientation factor, and J' is the spectral overlap integral. $F(\nu)$ is the normalized fluorescence spectrum of the energy donor, and $\epsilon(\nu)$ is the absorption spectrum of the energy acceptor with molar extinction coefficient (M^{-1} cm^{-1}). The distances (R) were estimated by the semiempirical PM3 calculation. The calculated energy hopping rates are 172 fs^{-1}, 6.7 ps^{-1}, and 246 fs^{-1} for the B states and 78 ps^{-1}, 3.1 ns^{-1}, and 111 ps^{-1} for the Q states of the *o*-dimer, *m*-trimer, and hexamer, respectively.[46] The values of the *o*-dimer and hexamer except the *m*-trimer are roughly consistent with the anisotropy decay times obtained by fluorescence upconversion and TCSPC techniques (Table 3). According to the Förster energy transfer, the energy-transfer rate shows inverse sixth power dependence on the center-to-center distance. Assuming that the distance between the adjacent porphyrin units in the *m*-trimer is 1.7 times longer than that of the *o*-dimer or hexamer, the Förster-type energy-transfer rate

in the *m*-trimer should be ~25 times slower. Despite the uncertainty in the energy hopping rate of the *m*-trimer described above, there exists a large discrepancy between the experimental energy-transfer rates and the calculated values. To explain such a large discrepancy, the electronic communication contribution through phenyl groups induced by π-electronic conjugation (through-bond interaction) is required, which is also consistent with the most red-shift of the B-band in the *m*-trimer in the absorption spectra of the arrays.

Finally, to gain further insight into the physics behind the fast depolarization process, it would be informative to know how large the coupling stengths are in our porphyrin arrays in relation to the LH1 and LH2 arrays in the natural photosynthetic system. The coupling strengths between Zn^{II}porphyrin moieties can be calculated from the observed excitation energy hopping rates as follows,[42]

$$\tau_{dep} = \frac{1}{\Gamma'}\frac{1}{1-A} \tag{13}$$

$$A = \frac{1}{N}\sum_{k=1}^{N}\frac{\Gamma'^2}{\Gamma'^2 + 16J^2\sin^2(2\pi/N)\sin^2(2\pi k/N)} \tag{14}$$

where Γ' and J are the homogeneous line width and the coupling strength, respectively. The homogeneous line widths of the *m*-trimer and hexamer were estimated to be ~600 cm^{-1} by a double-Gaussian fitting, which can be considered as the upper limit of the homogeneous line width. The B-band absorption line width of Zn^{II}TPP was reported to be ~250 cm^{-1} in ethanol glass at 103 K. Since the through-space interactions in our porphyrin systems are not so strong, this value can be used as a homogeneous line width for the porphyrin arrays. Figure 10 exhibits the results for the simulation of eqs 13 and 14 as Γ' is changed from 100 to 600 cm^{-1}, which indicates that it is important to know the exact Γ' value. The simulation results suggest that the intermolecular coupling strengths of the *m*-trimer and hexamer are ~95 and ~155 cm^{-1}, respectively, when Γ' is assumed to be 600 cm^{-1}. The J/Γ' value is less than 1, suggesting that these systems belong to the weak interaction regime, that is, the Förster regime. At $\Gamma' = 250$ cm^{-1}, the intermolecular coupling strengths of the *m*-trimer and hexamer are estimated to be 74 and 264 cm^{-1}, respectively. In this case, the J/Γ' value of the hexamer is ~1, which corresponds to the intermediate interaction regime. It is to be noted, however, that the Förster scheme is still well operative in explaining the EET processes of the hexamer. In light-harvesting pigment−protein complexes such as *Rs. molischianum* and *Rps. acidophila*, the dipole−dipole coupling strengths have been calculated based on the Förster equation. The intradimer (interdimer) coupling strengths of B850 in *Rs. molischianum* and *Rps. acidophila* were estimated to be 339 (336) and 322 (288) cm^{-1}, respectively, while those between B800 and between B800 and B850 were known to be in the range of 17−22 cm^{-1}.[1] It is noteworthy that the coupling strength between the B states in the hexamer is similar to that between the Q states in B850, while the coupling strength between the B states in the *m*-trimer is in a similar coupling strength regime to Q states in B800 of natural light-harvesting complexes. Since the nature and magnitude of the interactions in multiporphyrin systems are very important for applications in light emission and light harvesting, our porphyrin array systems have proven to be very promising in the framework of mimicking natural light-harvesting arrays.

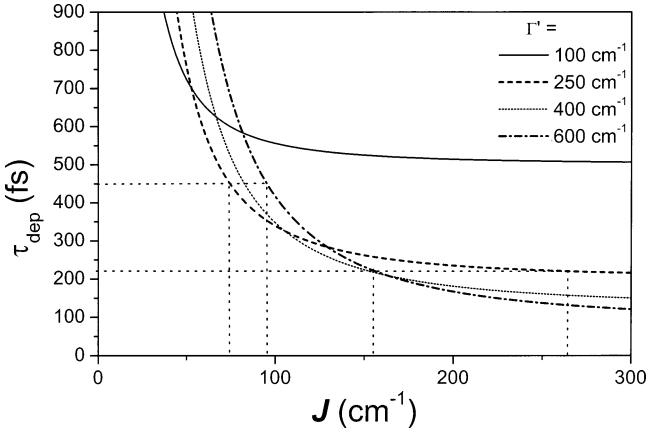

Figure 10. Simulations by eqs 13 and 14 showing that the intermolecular coupling constant can be estimated from the depolarization induced by the energy hopping dynamics. The homogeneous line width (Γ') was estimated to be in the range of 250~600 cm^{-1} from the Gaussian fitting of the B-band at low (103 K) and room temperature. Under this assumption, the intermolecular coupling constants are expected to be in range of the values for the *m*-trimer and hexamer.

Conclusions

We have measured energy-transfer and ultrafast internal conversion processes in the porphyrin arrays mimicking the natural photosynthetic light-harvesting antennas by utilizing time-resolved spontaneous fluorescence. The absorption and emission spectra of the porphyrin arrays were observed to be mostly unperturbed compared with their constituent monomer except for a slight change in the Soret band, which is well explained by the exciton coupling theory. The electronic interactions of the *o*-dimer and hexamer were described mainly by through-space dipole−dipole interactions, although an additional interaction term arising from through-bond interactions induced by π-conjugation should be introduced for *the m*-trimer. The internal conversion rates are accelerated in the order of *m*-trimer, *o*-dimer, and hexamer, which is expected to be closely related to the coupling strengths. From the fluorescence anisotropy decay dynamics of the arrays, we were able to determine the energy hopping rates between porphyrin moieties, and these values were compared with the calculation based on the Förster formula. Finally, we have estimated the inter-porphyrin coupling strengths of the porphyrin arrays from the energy hopping rates. The coupling strength between B states in the hexamer is slightly less than that between B850's and larger than that between B800's in the natural light-harvesting array system. Our observations illustrates that our porphyrin arrays are a well-

(46) It is difficult to evaluate the orientation factor because of the structural complexity of the porphyrin arrays. Therefore, these values were approximated to be 1, 0.66, and 0.7 for the *o*-dimer, *m*-trimer, and hexamer, respectively. In the *m*-trimer, the porphyrin moieties are assumed to be oriented relatively randomly because of enough space for the orientational motions between the adjacent porphyrins. The orientation factors of the *o*-dimer and hexamer were estimated from the coupling strengths shown in the absorption spectra, assuming that the inter-porphyrin geometries except the relative orientation are the same. The *R* values were evaluated to be ~10.6 Å for the *o*-dimer and hexamer and ~18.3 Å for the *m*-trimer. The spectral overlap integrals were calculated to be $\sim 3.5 \times 10^{-13}$ and $\sim 8.7 \times 10^{-15}$ cm^6 $mmol^{-1}$ for the B and Q states from the absorption and emission spectra of the monomer. The fluorescence lifetime (~2.5 ns) and quantum yield (~0.03) of the monomer were used. Especially, the natural radiative lifetime of the B state was estimated from the ratio between the absorption extinction coefficients of the B and Q states. The refractive index of toluene is ~1.5 at room temperature.

defined and promising system to mimic the natural light-harvesting arrays in view of molecular structure, constituent pigments, and coupling strengths between the adjacent chromophores.

Acknowledgment. This work has been financially supported by the National Creative Research Initiatives Program of the Ministry of Science & Technology of Korea (D.K.) and the National Research Laboratory program (T.J.) administered by KISTEP. The work at Kyoto was supported by Core Research for Evolutional Science and Technology (CREST) of Japan Science and Technology Corporation (JST).

Note Added after ASAP: The version of this paper published on the Web 4/19/2003 contained errors in eqs 3, 4, and 14. The final Web version published 4/29/2003 and the print version are correct.

JA021476G